Y. Lin, T. Riekkinen, W.-C. Li, E. Alon, and C. T.-C. Nguyen, "Metal micromechanical resonant switch for on-chip power applications," *Tech. Digest*, IEEE Int. Electron Devices Mtg., Washington, DC, Dec. 5-7, 2011, pp. 497-500.

A Metal Micromechanical Resonant Switch for On-Chip Power Applications

Yang Lin, Tommi Riekkinen, Wei-Chang Li, Elad Alon, and Clark T.-C. Nguyen

Berkeley Sensor & Actuator Center
Dept. of Electrical Engineering and Computer Sciences
University of California, Berkeley, California 94720 USA
Tel: (510)517-3931, Fax: (510)643-6637, Email: linyang@eecs.berkeley.edu

Abstract

A micromechanical resonant switch, or "resoswitch" (c.f., Fig. 1), constructed in nickel metal rather than previously used polysilicon attains a switch *FOM* >50 THz, which is several times higher than so far attained by power FET devices and pin diodes. Here, the use of metal reduces the "on" resistance of the resoswitch to less than 1Ω, allowing it to generate 17.7dB of sustained electrical power gain at 25MHz when embedded in a simple switched-mode power amplifier circuit, marking the first successful demonstration of RF power gain using a micromechanical resonant switching device. The high *FOM* of this device may soon permit the near 100% efficiency predicted for Class-E switched-mode power amplifiers that has eluded transistor-based versions for decades. This in turn would greatly extend battery lifetimes for portable wireless communications and other applications.

Introduction

Although improvements in transistor performance have certainly transformed the capabilities of digital circuits over the past few decades, they have had a much more measured effect on analog circuits. Indeed, in wireless circuits, the power amplifier (PA) remains a primary obstacle against longer battery lifetime, since PA efficiency over the years has improved relatively slowly. Among PA topologies, switched-mode ones like Class-E can theoretically achieve 100% drain efficiency, provided the switches used have sufficiently high figure of merit [$FOM = 1/(2\pi R_{on}C_{off})$, where R_{on} is on resistance, C_{off} is off capacitance]. Unfortunately, CMOS so far offers switch *FOM*'s less than 600GHz [1] with reasonable breakdown voltages; and even the GaAs HBT's commonly used in PA's only muster 3THz [2]. On the other hand, RF MEMS switches [3] attain much higher *FOM* >60THz, so would be ideal for PA's if not plagued by issues like low switching speed, large actuation voltage, and poor reliability.

Pursuant to circumventing these issues, the micromechanical resonant switch ("resoswitch") introduced in [4] harnesses the resonance and nonlinear dynamical properties of its mechanical structure to greatly increase switching speed and cycle count (even under hot switching), and lower the needed actuation voltage, all by substantial factors over existing RF MEMS switches, making it suitable for high efficiency power amplifier applications. The switch of [4], however, was constructed in doped polysilicon, which compromised its ability to achieve power gain, since its high series and contact resistances loaded down its *FOM*. This work overcomes the problem by constructing the resoswitch in nickel metal to attain a switch *FOM* greater than 50 THz, which is several times higher than so far attained by power FET devices and pin diodes [5]. Here, the use of metal reduces the "on" resistance of the resoswitch to less than 1Ω, allowing it to generate 17.7dB of sustained electrical power gain at 25 MHz when embedded into the simple switched-mode PA circuit of Fig. 1, marking the first successful demonstration of RF power gain using a micromechanical resonant switching device.

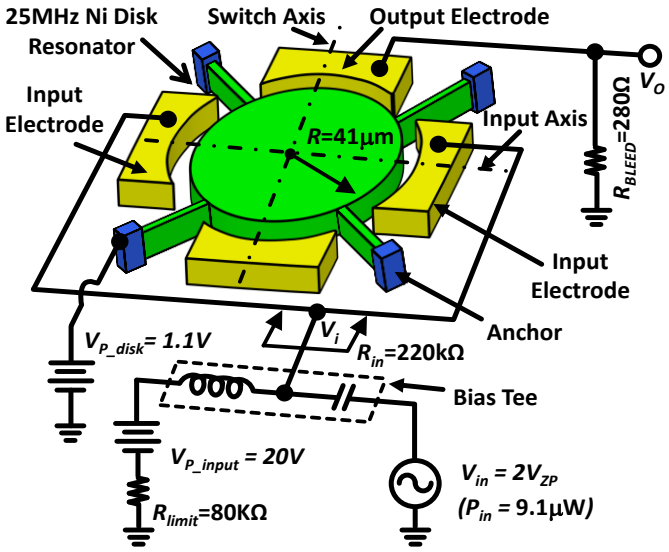

Fig. 1: Schematic of the micromechanical resonant switch in a simple switched-mode power amplifier circuit.

Device Structure and Operation

Fig. 1 presents a schematic of the metal resoswitch in the simple circuit used to demonstrate switched-mode power gain. As shown, the device consists of a 41μm-radius Ni disk designed to mechanically vibrate at 25 MHz in the wine-glass mode shape shown in Fig. 2, where the disk expands and contracts along orthogonal axes. The disk is suspended 700 nm above a TiNi/Ni metal ground plane (attached to the substrate) by four support beams located at nodes in the mode shape to minimize energy loss to the substrate. Ni electrodes surround the disk, spaced 120 nm from its edges along the input axis, i.e., along the axis where the input drive signal is applied; and 80 nm along the orthogonal switching axis, i.e., the axis along which the disk contacts the output electrodes.

A 2V zero-to-peak sinusoid near the disk resonance frequency applied to the input electrodes is sufficient to drive

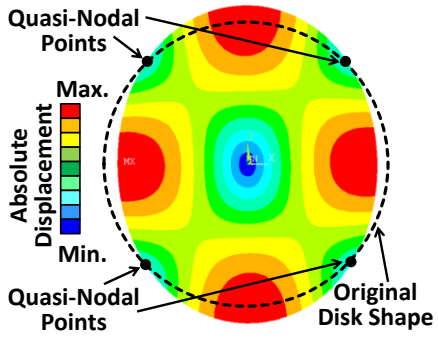

Fig. 2: Finite element simulated wine-glass disk mode shape, in which the disk expands and contracts along orthogonal axes.

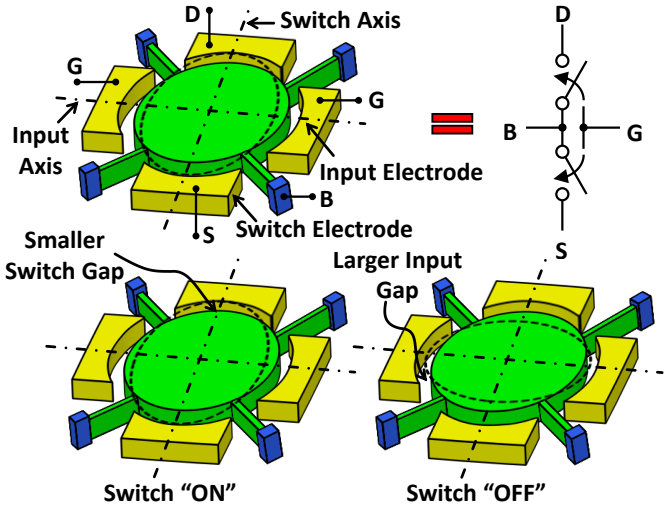

Fig. 3: Schematic depicting impacting in the wine-glass mode resoswitch along the switch axis, but not along the input axis.

the disk so that it impacts the electrodes along the switch axis, but not along the larger gapped input axis, as shown in Fig. 3. Periodic switching thus ensues as vibration of the disk opens and closes the contact with a period and duty cycle set by the frequency and amplitude of the input signal.

Operation at resonance provides many advantages over non-resonant switches. In particular, because resonance operation effectively multiplies the displacement amplitude by the system *Q*, which can be in the thousands, a resoswitch can be designed with a much larger stiffness on the order of 1.6 MN/m, compared with the 50 N/m of a typical conventional MEMS switch, while also reducing the actuation voltage to a more reasonable value. The large stiffness of a resoswitch in turn allows it to operate at much higher frequency than a conventional MEMS switch while simultaneously improving reliability, since the higher stiffness now generates a much larger force with which to overcome stiction forces. In addition to these benefits, impacting operation actually expands the bandwidth of the resonant switch, as shown in Fig. 11 of [6], allowing the device to amplify over a bandwidth much larger than that of a non-impacting resonator. In fact, as the peak flattens it spreads out over a larger bandwidth. Effectively, the amplifying bandwidth of the resoswitch is a function of the drive voltage, so can be controlled at will.

a) Deposit TiNi/Ni interconnect layer, deposit bottom sacrificial layer and pattern disk anchors, electroplate nickel structural layer and Cu spacer layer using photoresist (PR) mold.

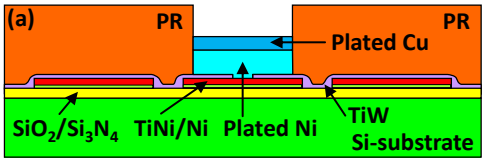

b) Deposit sidewall sacrificial layer and pattern electrode anchors, and then electroplate surrounding electrodes through PR mold.

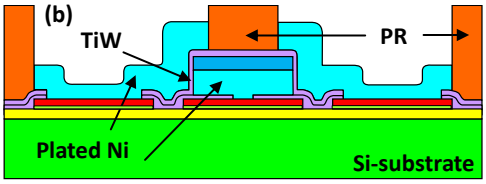

c) Wet release.

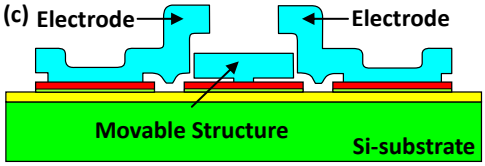

Fig. 4: Surface-micromachining fabrication process for the nickel resoswitch.

Of course, operation at resonance constrains this switch to applications that require periodic switching, which makes it unsuitable for digital logic or antenna switching. Fortunately, the majority of power applications, e.g., power amplifiers and power converters, require periodic switching, and these applications are arguably much more lucrative, since it is in these where existing on-chip devices are most lacking.

Fabrication Process

Pursuant to confirming the benefits of resonance operation, plus demonstrate power gain, Fig. 4 presents the process flow used to fabricate nickel metal resoswitches with the design of Fig. 1. The process begins with successive LPCVD depositions of SiO_2 and low stress Si_xN_y at 450°C and 835°C, respectively, to provide electrical isolation from the conductive silicon substrate. (Note that these layers are not needed when fabricating above CMOS.) Successive films of 5 nm of TiNi alloy adhesion layer and 100 nm of Ni are then sputtered and patterned via liftoff to form electrical interconnects. Next, 700 nm of TiW is blanket sputter deposited to serve as a bottom sacrificial layer that temporarily supports structures to be released later. Anchor vias are then plasma etched into the TiW using an SF_6+O_2 chemistry, followed by O_2 plasma cleaning of residues formed during dry etching to improve structure-to-interconnect contact. Next, the Ni structural layer is electroplated 3μm-thick into the open spaces of a 6μm photoresist mold defining the resonator disks and support beams. Cu is then electroplated using the same mold to yield Fig. 4(a) and to serve as a capping layer over all structures that separates the eventual electrodes from the tops of the disks.

A second film of TiW, this time 80 or 120 nm-thick (depending on direction), is blanket sputter deposited to serve as

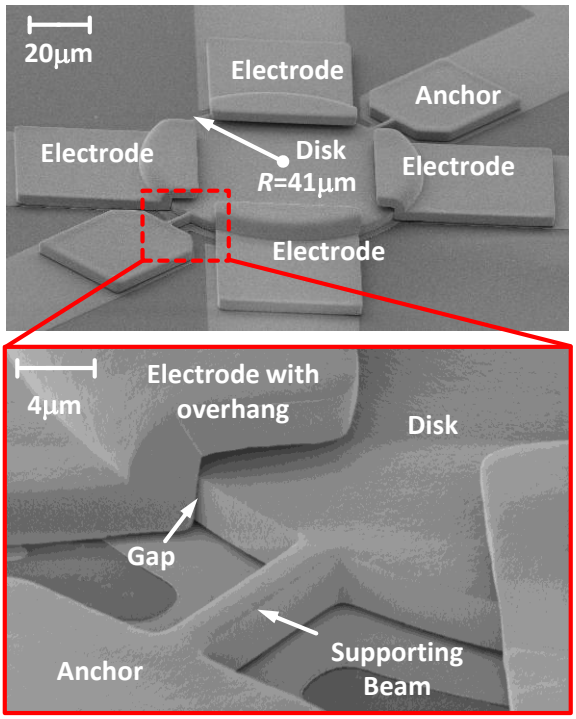

Fig. 5: SEM of a 25-MHz wine-glass mode electroplated-nickel disk resonant switch, with zoom in on an anchor and on the electrode-to-disk gap.

a sidewall sacrificial layer that defines the gap spacing between the electrodes and the resonator disk. This sputtering step is surprisingly conformal over the sides of the disks, but fortuitously, not completely isotropic. In particular, proper orientation of the wafer in the sputtering chamber permitted deposition of different thicknesses along the different axes of the disk, allowing this process to realize the unequal input and switch axis electrode-to-resonator gaps needed for proper switch operation [7] [8]. After the gap-defining deposition, anchors for the electrodes are patterned and etched into the total TiW layer, and electrodes surrounding the disk are electroplated through a 2nd photoresist mold to yield Fig. 4(b). Finally, the TiW sacrificial layer is removed via a $NH_4(OH)+H_2O_2$ wet etch in the very last step of the process to free devices and yield Fig. 4(c).

Fig. 5 presents the SEM of a 25-MHz nickel disk resoswitch resulting from this process, with a zoom in on a support beam that also includes one of the tiny disk-to-electrode gaps. Since temperatures (after the isolation layers, which aren't needed when fabricating over CMOS) never exceed 100°C, the process of Fig. 4 is quite compatible with CMOS, so can potentially enable a single-chip RF transmitter solution, where CMOS up-conversion circuits precede a highly efficient resoswitch-based power amplifier.

Experimental Results

The power gain circuit of Fig. 1 is very similar in structure to that of an equivalent transistor version shown in Fig. 6. In the resoswitch version, a dc-bias voltage $V_{P,input}$ (which could also just be dc charge) and an ac voltage at resonance v_{in}

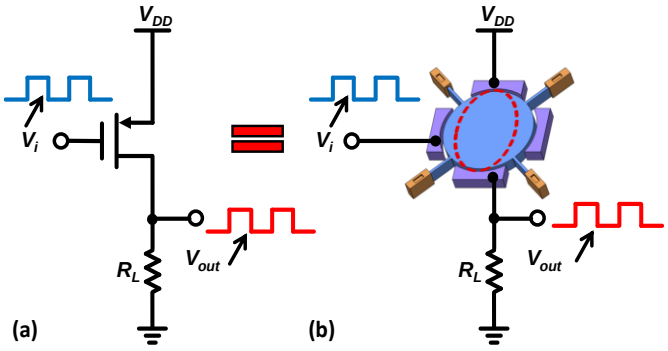

Fig. 6: Comparison of power gain circuit schematics using (a) a transistor switch; and (b) a micromechanical resoswitch.

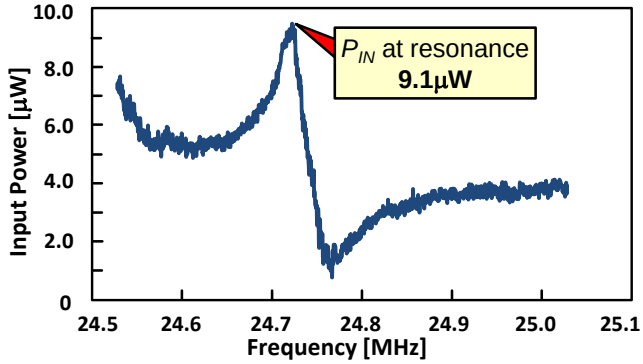

Fig. 7: Input power as a function of frequency measured by a network analyzer at node V_i in Fig. 1 and used to determine input impedance.

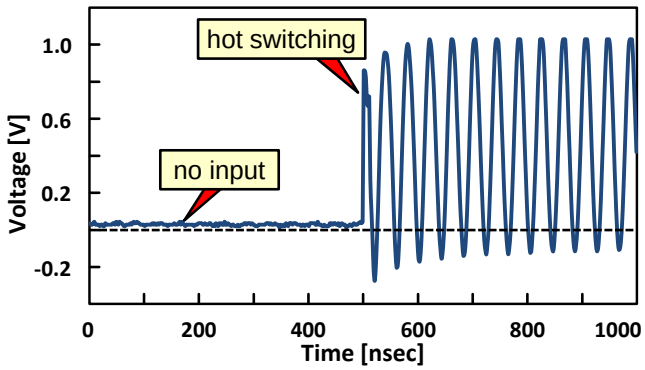

Fig. 8: Output waveform at node V_o in Fig. 1, measured using an oscilloscope.

combine at the input electrode to generate a force within the resonator passband that drives the disk into vibration with the mode shape of Fig. 2. When v_{in} is given a zero-to-peak amplitude of 2V, the disk amplitude becomes large enough to impact its electrodes along the switch axis, thereby making electrical contact and transferring power from the $V_{P,disk}$ = 1.1V supply to the output load R_{bleed}.

Fig. 7 and Fig. 8 plot the measured input power spectrum (on a network analyzer) and output waveform (on an oscilloscope), respectively, taken at the same time under a vacuum of 25μTorr. Note how the input power peaks at resonance, where the input impedance is minimized. Although the input zero-to-peak voltage amplitude of 2V is larger than the 0.55V at the output node, there is still power gain, since the output

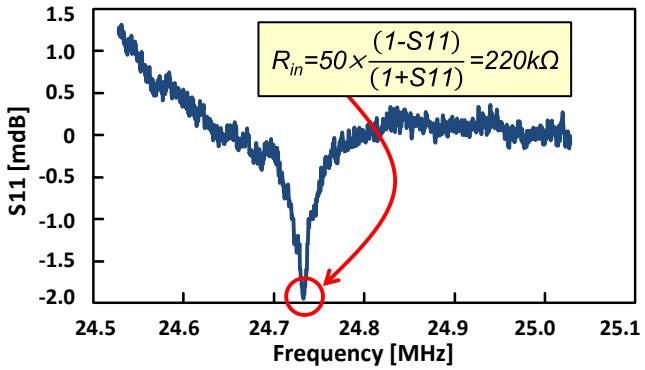

Fig. 9: Measured S11 used to extract the resoswitch input resistance.

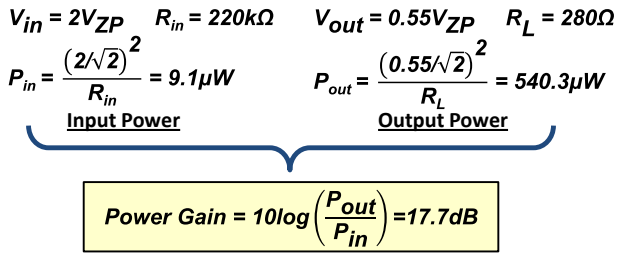

Fig. 10: Explicit calculation of the input power, output power, and power gain, delivered by the resonant switch in the switched-mode power amplifier circuit of Fig. 1.

impedance is much smaller than the input impedance. In particular, the output impedance is merely the 280Ω load, and the input impedance is 220kΩ, as measured in the S11 plot of Fig. 9. Fig. 10 explicitly calculates the power gain to be 17.7dB, which is quite respectable. The input power is 9.1μW, and this is amplified to 0.54mW delivered to the 280Ω output load.

The power gain generated by the simple power amplifier circuit of Fig. 1 comes about mainly due to the small on resistance R_{on} of the metal resoswitch, which at a measured 0.5Ω is much smaller than the 1.1kΩ of a previous resoswitch made of doped polysilicon material [4]. The small R_{on} combines with a tiny off capacitance C_{off}, estimated at ~7fF, to achieve an impressive *FOM* of 50 THz. Table 1 compares the demonstrated metal resoswitch with its MEMS predecessor and with a top semiconductor FET contender [9]. Clearly, the metal resoswitch of this work bests the semiconductor by orders of magnitude in *FOM*, which is the main parameter that governs performance in power amplifiers and converters.

The output waveform shown in Fig. 8 lasts for 200 million cycles, at which point instabilities pull the device into its electrode [14] (but do not destroy it, as it is actually recoverable). Defensive design to prevent pull-in should be possible in future renditions of this device. For example, instead of creating different disk-to-electrode gaps at input and output, the displacement amplifier designs described in [7] and [8] employing mechanical stiffness engineering to generate larger displacements at the output disk than the input, can prevent input impacting in a more repeatable and effective way. Furthermore, removing electrode overhangs via the etch-back process introduced in [15] increases the dc pull-in voltage, thereby helping to stabilize the device during switching.

Table 1: Comparison of Power Switch Technologies

Parameter	FET Switch	Conventional MEMS Switch	Metal Resoswitch
Actuation Voltage (V)	1-3	20-80	2
Switching time	0.16-1ns[9]	1-300μs	~10ns
Life time (# cycles)	Very large	100 Billion[11]	200 Million
Off State Power	0.2-3 μW	0	0
On Resistance R_{ON} (Ω)	0.5[10]	0.1-1[12]	~0.5
Input Capacitance	~20pF[10]	1-10fF[13]	7fF
$FOM=1/(2\pi R_{ON}C_{off})$	590 GHz [1]	63 THz	>50THz

Conclusions

The use in this work of a CMOS-compatible process to realize a 25-MHz wine-glass disk resoswitch in nickel structural material greatly reduces switch on resistance relative to previous polysilicon versions towards an *FOM* greater than 50 THz and a measured power gain of 17.7dB when emplaced into a simple switch-mode amplifier circuit. The demonstrated power gain, although ample, is not the most efficient possible, since the circuit used to generate it is not Class E. To realize Class E operation and perhaps get closer to its theoretical 100% efficiency, energy storage elements, i.e., inductors and capacitors, must be added at proper locations and in proper amounts. Work towards this continues.

Acknowledgment. This work was supported by the DARPA NEMS program.

References

[1] I. Aoki, *et al.*, "A Fully Integrated Quad-Band …," in *IEEE ISSCC 2008, Digest of Technical Papers*, Feb. 3-7, 2008, pp. 570-636.
[2] D.A. Blackwell, *et al.*, "X-band MMIC switch with …," in *IEEE μwave and mm-Wave Monolithic Ckts. Symp., Digest of Papers*, May 12-16, 1995, pp. 97-100.
[3] Z. Yao, *et al.*, "Micromachined low-loss …," *IEEE/ASME J. Microelectromechanical Systems*, vol.8, no.2, pp. 129-134, June 1999.
[4] Y. Lin, *et al.*, "The micromechanical resonant switch ..., " in *Technical Digest*, Hilton Head 2008, South Carolina, June 1-5, 2008, pp. 40-43.
[5] Putnam, *et al.*, "A monolithic GaAs …," in *IEEE Radio Frequency Intg. Ckts (RFIC) Symp.*, June 8-11, 1997, pp. 225-228.
[6] Y. Lin, *et al.*, "A resonance dynamical approach …," in *Proc.* 2008 *IEEE Int. Freq. Ctrl. Symp.*, May 19-21, 2008, pp. 640-645.
[7] Y. Lin, *et al.*, "Digitally-specified micromechanical …," in *Dig. of Tech. Papers, TRANSDUCERS'09*, June 21-25, 2009, pp. 781-784.
[8] B. Kim, *et al.*, "Micromechanical Resonant Displacement Gain Stages," in *Technical Digest, IEEE MEMS'09*, Jan. 25-29, 2009, pp. 19-22.
[9] H. Kamitsuna, *et al.*, "A fast low-power …," in *Proc., IEEE Compound Semiconductor IC Symp.*, Oct. 24-27, 2004, pp. 97- 100.
[10] Agilent Technologies, "Agilent solid state …," 2007.
[11] S. Majumder, *et al.*, "A packaged, high-lifetime …," in *μwave Sym. Dig., IEEE Int. MTT-S 2003*, vol.3, pp. 1935- 1938, June 8-13, 2003.
[12] J. B. Muldavin, *et al.*, "High-isolation inductively- …," in *μwave Sym. Dig., IEEE Int. MTT-S 2000*, vol.1, pp. 169-172, June 11-16, 2000.
[13] G. M. Rebeiz, *et al.*, "RF MEMS switches and switch circuits," *IEEE Microwave Magazine*, vol.2, no.4, pp. 59-71, Dec. 2001.
[14] H.C. Nathanson, *et al.*, "The resonant gate transistor," *IEEE Transactions on Electron Devices*, vol.14, no.3, pp. 117- 133, Mar 1967.
[15] J.R. Clark, *et al.*, "High-Q UHF …," *IEEE/ASME J. Microelectromechanical Systems*, vol.14, no.6, pp. 1298- 1310, Dec. 2005.